

Bachelor Thesis



**Czech
Technical
University
in Prague**

F4

**Faculty of Nuclear Sciences and Physical Engineering
Department of Physics**

Machine Learning-Driven Nonlocal Hydrodynamics for Thermonuclear Fusion Modeling

Aleksandr Bogdanov

Supervisor: Ing. Milan Holec, Ph.D.

Consultant: doc. Ing. Pavel Váchal, Ph.D.

Study Programme: Physical Engineering

Specialization: Plasma Physics and Thermonuclear Fusion

July 2023



BACHELOR THESIS ASSIGNMENT

Academic year: 2022/2023

Student: Aleksandr Bogdanov

Study programme: Physical Engineering

Specialization: Physics of Plasma and Thermonuclear Fusion

Thesis title: Aplikace strojového učení při nelokálním hydrodynamickém modelování termojaderné fúze
(in Czech)

Thesis title: Machine Learning-Driven Nonlocal Hydrodynamics for Thermonuclear Fusion Modeling
(in English)

Language of the Thesis: English

Instructions:

- 1) Get acquainted with the state-of-the-art inertial confinement fusion (ICF) research and the importance of the physical phenomena of transport [1, 2, 3].
- 2) Research hydrodynamic models currently used in ICF with the focus on nonlocal electron transport [4].
- 3) Process kinetic modeling data provided by Lawrence Livermore National Laboratory.
- 4) Teach a deep neural network (DNN) to learn the process of nonlocal electron transport based on physically motivated loss function [5, 6, 7].
- 5) Compare the DNN model with the classical heat flux limiter model used in ICF [8].

Recommended literature:

- [1] H. Abu-Shawareb et al. (Indirect Drive ICF Collaboration), "Lawson Criterion for Ignition Exceeded in an Inertial Fusion Experiment", *Physical Review Letters* 129, 075001 (2022).
- [2] D. T. Casey, et al., "Evidence of Three-Dimensional Asymmetries Seeded by High-Density Carbon-Ablator Nonuniformity in Experiments at the National Ignition Facility", *Physical Review Letters* 126, 025002 (2021).
- [3] M. D. Rosen, et al., "The role of a detailed configuration accounting (DCA) atomic physics package in explaining the energy balance in ignition-scale hohlraums", *High Energy Density Physics* 7 (3), 180-190 (2011).
- [4] M. Holec, J. Nikl and S. Weber, "Nonlocal transport hydrodynamic model for laser heated plasmas", *Physics of Plasmas* 25, 032704 (2018).
- [5] PyTorch Lightning Tutorial, <https://becominghuman.ai/pytorch-lightning-tutorial-1-getting-started-5f82e06503f6>.
- [6] Introduction to PyTorch Lightning, <https://pytorch-lightning.readthedocs.io/en/stable/>
- [7] Regression using PyTorch Lightning, "Bike Share Regression PyTorch Lightning.ipynb", <https://github.com/shotleft/how-to-python.git>.
- [8] D. A. Chapman, et al., "A preliminary assessment of the sensitivity of uniaxially driven fusion targets to flux-limited thermal conduction modeling", *Physics of Plasmas* 28, 072702 (2021).

Name and affiliation of the supervisor:

Ing. Milan Holec, Ph.D.

Lawrence Livermore National Laboratory, CA, USA

Name and affiliation of the consultant:

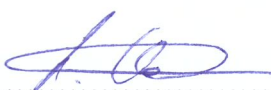
doc. Ing. Pavel Váchal, Ph.D.

Department of Physical Electronics, Faculty of Nuclear Sciences and Physical Engineering
CTU in Prague

Date of the assignment: 20.10.2022

Due date of the thesis: 02.08.2023

The assignment is valid for two years since the ~~date~~ of the assignment


.....
Guarantor of the study programme




.....
Department head


.....
Dean

In Prague on 20.10.2022

ZADÁNÍ BAKALÁŘSKÉ PRÁCE

Akademický rok: 2022/2023



Student: Aleksandr Bogdanov

Studijní program: Fyzikální inženýrství

Specializace: Fyzika plazmatu a termojaderné fúze

Název práce: Aplikace strojového učení při nelokálním hydrodynamickém
(česky) modelování termojaderné fúze

Název práce: Machine Learning-Driven Nonlocal Hydrodynamics for Thermonuclear
(anglicky) Fusion Modeling

Jazyk práce: Angličtina

Pokyny pro vypracování:

V rámci bakalářské práce proveďte následující úkony:

- 1) Seznamte se se současným stavem a nejnovějšími poznatky z oblasti výzkumu inerciální termojaderné fúze (ICF) a důležitostí fyzikálního jevu tzv. transportu [1, 2, 3].
- 2) Proveďte rešerši hydrodynamických modelů používaných pro simulace fúzních experimentů, zaměřte se především na nelokální elektronový transport [4].
- 3) Zpracujte data získaná z kinetických modelů v Lawrence Livermore National Laboratory.
- 4) Naučte hlubokou neuronovou síť (DNN) učit se proces nelokálního transportu na základě správně definované, fyzikálně motivované ztrátové funkce [5, 6, 7].
- 5) Porovnejte model neuronové sítě s klasickým modelem limiteru tepelné vodivosti používaným pro ICF [8].

Doporučená literatura:

- [1] H. Abu-Shawareb et al. (Indirect Drive ICF Collaboration), "Lawson Criterion for Ignition Exceeded in an Inertial Fusion Experiment", Physical Review Letters 129, 075001 (2022).
- [2] D. T. Casey, et al., "Evidence of Three-Dimensional Asymmetries Seeded by High-Density Carbon-Ablator Nonuniformity in Experiments at the National Ignition Facility", Physical Review Letters 126, 025002 (2021).
- [3] M. D. Rosen, et al., "The role of a detailed configuration accounting (DCA) atomic physics package in explaining the energy balance in ignition-scale hohlraums", High Energy Density Physics 7 (3), 180-190 (2011).
- [4] M. Holec, J. Nikl and S. Weber, "Nonlocal transport hydrodynamic model for laser heated plasmas", Physics of Plasmas 25, 032704 (2018).
- [5] PyTorch Lightning Tutorial, <https://becominghuman.ai/pytorch-lightning-tutorial-1-getting-started-5f82e06503f6>.
- [6] Introduction to PyTorch Lightning, <https://pytorch-lightning.readthedocs.io/en/stable/>
- [7] Regression using PyTorch Lightning, "Bike Share Regression PyTorch Lightning.ipynb", <https://github.com/shotleft/how-to-python.git>.
- [8] D. A. Chapman, et al., "A preliminary assessment of the sensitivity of uniaxially driven fusion targets to flux-limited thermal conduction modeling", Physics of Plasmas 28, 072702 (2021).

Jméno a pracoviště vedoucího bakalářské práce:

Ing. Milan Holec, Ph.D.

Lawrence Livermore National Laboratory, CA, USA

Jméno a pracoviště konzultanta:


doc. Ing. Pavel Váchal, Ph.D.


Katedra fyzikální elektroniky, Fakulta jaderná a fyzikálně inženýrská ČVUT v Praze

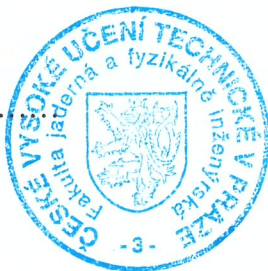
Datum zadání bakalářské práce: 20.10.2022

Termín odevzdání bakalářské práce: 02.08.2023

Doba platnosti zadání je dva roky od data zadání.


.....
garant studijního programu


.....
vedoucí katedry




.....
Děkan

V Praze dne 20.10.2022

ČESKÉ VYSOKÉ UČENÍ TECHNICKÉ V PRAZE

Fakulta jaderná a fyzikálně inženýrská

Břehová 7
115 19 Praha 1



PROHLÁŠENÍ

Já, níže podepsaný

Jméno a příjmení studenta: Aleksandr Bogdanov

Osobní číslo: 502470

Název studijního programu (oboru): Fyzikální inženýrství - FPTF

prohlašuji, že jsem bakalářskou práci s názvem:

Aplikace strojového učení při nelokálním hydrodynamickém modelování termojaderné fúze

vypracoval samostatně a uvedl veškeré použité informační zdroje v souladu s Metodickým pokynem o dodržování etických principů při přípravě vysokoškolských závěrečných prací.

V Praze dne 31.07.23

.....
podpis

Acknowledgements

I would like to express my sincere gratitude to Milan Holec for supervising my thesis and providing invaluable help and support throughout the process. Additionally, I extend my thanks to Pavel Váchal for his important comments on the thesis formatting and his overall assistance with administrative matters. Lawrence Livermore National Laboratory did not provide any modeling data and previously published IMPACT kinetic data has been used in our work.

Declaration

I declare that this work is all my own work and I have cited all sources I have used in the bibliography.

Prague, 31. July 2023

Abstract

The interactions in laser heated plasma often take place under non local transport conditions, when predictions of classic diffusive models give inaccurate results. When high gradients of temperature and density are present, heat propagates not only by spreading the collisions of relatively slow moving particles. Fast moving particles such as electrons could escape the region of high density, thus carrying out significant amount of energy. The purpose of this work is to introduce the reader to the concept of non-local heat transport in laser heated plasma, and describe key moments of a neural network model, purpose of which is to predict behavior of heat flux inside hohlraums used at the National Ignition Facility.

Keywords: plasma, laser, nonlocal electron transport, neural network, heat transport

Supervisor: Ing. Milan Holec, Ph.D.
7000 East Ave., Livermore, California,
USA

Abstrakt

Interakce v laserem ohřátém plazmatu často probíhají za podmínek tzv. nelokálního transportu elektronů, kdy předpovědi klasického difuzního modelu dávají nepřesné výsledky. Za přítomnosti velkých gradientů teploty a hustoty plazmatu se teplo šíří nejen prostřednictvím srážek relativně pomalých částic. Rychle se pohybující částice (např. elektrony) jsou schopny opustit oblast vysoké hustoty a tím odnést z této oblasti značné množství energie. Cílem této práce je seznámit čtenáře s koncepcí nelokálního transportu tepla v laserem ohřátém plazmatu a popsat klíčové momenty modelu neuronové sítě, která předpovídá chování tepelného toku uvnitř hohlraumu, jenž je používán v National Ignition Facility.

Klíčová slova: plazma, laser, nelokální transport elektronů, neuronová síť, přenos tepla

Překlad názvu: Aplikace strojového učení při nelokálním hydrodynamickém modelování termojaderné fúze

Contents

Introduction	1
1 Introduction to Inertial Confinement Fusion and Transport Phenomena	3
1.1 Radiation hydrodynamic model of inertial confinement fusion	4
2 State-of-the-Art of Nonlocal Electron Transport	7
2.1 Kinetic models	8
2.2 Spitzer-Härm	9
2.3 Heatflux limiter	10
2.4 Convolution LMV and SNB models	11
3 Machine Learning-Driven Hydrodynamic Closure	13
3.1 Data preparation	14
3.2 Multilayer perceptron	15
3.3 Novel nonlocal thermal transport model	17
3.3.1 Newton's iteration	22
3.3.2 Boundary conditions	23
4 Results	25
5 Conclusions	31
Bibliography	33

Figures

3.1 Profiles of the initial data and construction of data vector. Each profile contains 400 datapoints. . . .	14
3.2 The representative scheme of MLP structure.	17
3.3 Profile of neural network prediction compared to kinetic reference IMPACT.	18
3.4 ∇q profile of neural network prediction compared to kinetic reference IMPACT.	19
3.5 Nonlocal heat flux within the expanding hohlraum wall	20
3.6 Self-similar "conductive nonlinearity" exhibited by preheat.	21
3.7 Discretization of the 1D problem	21
4.1 Time evolution of T according to MLP solver	26
4.2 Time evolution of T according to SH heatflux (2.10)	26
4.3 Time evolution of T according to heatflux limiter (2.12)	26
4.4 Comparison of the final profiles ($t=0.4$ ns) of the solutions.	27
4.5 Comparison of coefficients α given by MLP and heatflux limiter respectively	28
4.6 Comparison of the final profiles given by 18 separately trained MLPs	28
4.7 Deviation of the 70 separately trained MLPs	29
4.8 Time evolution of heatflux q_{MLP}	29



■ Introduction

Due to the fact that humanity has been trying to achieve the stability of the thermonuclear process for more than half a century, many technical solutions to this physical problem have been proposed during this time. One of such solutions is the design of inertial fusion, where capsules containing deuterium and tritium are irradiated by laser beams and thus implode in a central hot spot. Experiments with inertial fusion are being conducted in the Lawrence Livermore National Laboratory, where significant improvements have been made to this design [1, 2, 3].

Predicting the plasma behavior in laser heated plasma is a complex problem, that can't be solved without numerical implementation of a model, that should adequately bring us closer to the physical context of heat transport. Often it is done using magneto-hydrodynamics models [4, 5], frequently implemented numerically [6, 7].

The well known and the most popular model which can describe transport of heat is so-called diffusive model, also known as Fourier law $\mathbf{q} = k\nabla T$, which says that magnitude of heat flux is directly proportional to temperature gradient. Unfortunately, as a price for its simplicity, this approach becomes inaccurate in case of nonlocal electron transport discussed in this thesis.

Our approach is to predict heat flux, occurring under non-local transport in hohlraum, using feed forward Multilayer Perception (MLP). With this we expect significantly faster calculation of heatflux \mathbf{q} and consequently better performance of simulations of time evolution of plasma temperature. It is worth mentioning, that recently an Artificial Neural Network (ANN) predicting heatflux was used and compared with SNB approach (see Section 2.4) in the article of Lamy et al. [8], where ANN was applied in several cases of laser driven ablation of a plastic target.

The rest of this thesis is organized as follows: In the first chapter, the basics of Inertial Confinement Fusion (ICF) and transport theory are presented. This is followed by the second chapter, where a few popular kinetic and hydrodynamic models are discussed. The third chapter describes our MLP model and the method of implementing time evolution of the temperature profile using the Newton Implicit method. The results of the work are presented in the fourth chapter, where our MLP model is compared with two different hydrodynamic models previously discussed in the second chapter. Finally, the thesis concludes with a summary of findings.

Chapter 1

Introduction to Inertial Confinement Fusion and Transport Phenomena

Inertial confinement fusion (ICF) is an approach to achieve controlled nuclear fusion, which has the potential to provide abundant and clean energy for the future. It involves using high-energy lasers or particle beams to compress and heat a target containing fusion fuel, typically in the form of small pellets or capsules. The intense pressure and temperature generated in the process aim to initiate a self-sustaining fusion reaction.

The fundamental principle behind ICF is to create conditions similar to those found in the core of stars, where nuclei fuse together releasing a significant amount of energy. By confining and compressing the fuel to high densities and temperatures, fusion reactions can occur, leading to the release of large amounts of energy. Under these conditions the fusing matter stays in the state of plasma - an aggregate state, which is characterized by its specificity to stay quasineutral (the sum of charges in plasma as a whole is roughly zero, although locally it may be charged) and perform collective behavior, e.g. shielding charges of individual particles [9].

In order for the reactions to be self-sustainable, a condition called the Lawson criterion has to be fulfilled within plasma inside the confinement device [3]. Lawson criterion describes circumstances at which fusion self-heating power just balances losses from bremsstrahlung x-ray radiation. Generally, the Lawson criterion represents an inequality, one side of which is a product of fusing nuclei' density n and confinement time τ , and the other side is an expression dependent on kinetic energy of particles (which is proportional to the temperature of plasma T), reactivity section $\langle\sigma v\rangle$ and energy ε , that releases as a result of fusion reaction.

Early researchers recognized that the most favored fusion reaction is deuterium(D) – tritium(T) fusion $D+T \longrightarrow n(14.1\text{MeV}) + {}^4\text{He}(3.5\text{MeV})$ because it has the largest reactivity for relatively low temperature ≈ 4.3 keV. For D-T

distribution function f_α due to collisions with ions, and this is what is the greatest difficulty in solving this equation.

As was discussed in the beginning of this section, working directly with kinetic equations is a rather laborious process and in some cases the accuracy of solutions will not suffer from certain simplifications. One of such simplifications are the generally accepted equations of fluid dynamics, derived as moments of the equation (1.2). More about models using kinetic theory will be written at the beginning of the next section. Here we will prepare the theoretical basis of fluid dynamics.

The equations of fluid dynamics comprise conservation laws of mass, momentum, and energy. We consider collision interactions only between electrons, i.e. $f_e = f_\alpha = f_\beta$.

Let us first define some summational invariant for which the following applies

$$\psi_\alpha + \psi_\beta = \psi'_\alpha + \psi'_\beta, \quad (1.3)$$

where ψ'_α and ψ'_β represents the value of ψ_α and ψ_β after collision. Then for any such function ψ the following also applies [11]

$$\sum_{\alpha,\beta} \int \psi_\alpha \left(\frac{df_\alpha(\mathbf{v}_\alpha)}{dt} \Big| f_\beta \right)_{coll} d^3\mathbf{v}_\alpha = 0, \quad (1.4)$$

where we also used $\psi_\alpha = \psi_\beta$.

If we multiply Boltzmann transport equation by a velocity dependent summational invariant $\psi_\alpha(\mathbf{v})$ related to particle of type α and integrate it over the velocity space d^3v , the conservation theorem can be written as

$$\begin{aligned} & \frac{\partial}{\partial t} (n_\alpha \langle \psi_\alpha(\mathbf{v}_\alpha) \rangle_\alpha) + \nabla_{\mathbf{x}} \cdot (n_\alpha \langle \psi_\alpha(\mathbf{v}_\alpha \mathbf{v}_\alpha) \rangle_\alpha) - \\ & - \frac{n_\alpha q_\alpha}{m_\alpha} \langle (\mathbf{E} + \mathbf{v}_\alpha \times \mathbf{B}) \cdot \nabla_{\mathbf{v}} \psi_\alpha(\mathbf{v}_\alpha) \rangle_\alpha = \int \psi_\alpha \sum_{\beta,\alpha} \left(\frac{df_\alpha}{dt} \Big| f_\beta \right)_{coll} d^3v_\alpha. \end{aligned} \quad (1.5)$$

If for ψ_α we substitute the following five collisional invariants

$$\psi_{\alpha 1} = m_{\alpha 1}, \quad \psi_{\alpha 2} = m_\alpha v_{\alpha 1}, \quad \psi_{\alpha 3} = m_\alpha v_{\alpha 2}, \quad \psi_{\alpha 4} = m_\alpha v_{\alpha 3}, \quad \psi_{\alpha 5} = \frac{m_\alpha}{2} |\mathbf{v}_\alpha|^2, \quad (1.6)$$

we obtain the equation of continuity, the three equations of momentum, and the energy equation for the field.

$$\frac{d\rho}{dt} = -\rho \nabla \cdot \mathbf{u}, \quad (1.7a)$$

$$\rho \frac{d\mathbf{u}}{dt} = -\nabla p, \quad (1.7b)$$

$$\rho \frac{d\varepsilon}{dT} \frac{dT}{dt} + \frac{d\varepsilon_R}{dt} = \left(\rho^2 \frac{\partial \varepsilon}{\partial \rho} - p \right) \nabla \cdot \mathbf{u} - \nabla \cdot (\mathbf{q}_H + \mathbf{q}_R) + Q_{IB}, \quad (1.7c)$$

Chapter 2

State-of-the-Art of Nonlocal Electron Transport

In this chapter I will first introduce the basis of currently used kinetic models, and in the second part of the chapter the most commonly used hydrodynamic closures will be discussed. The key equation to describe transport of particles is the Boltzmann's equation. We consider the Lorentz force as the only force acting on individual particles. Boltzmann's equation in this case reads

$$\frac{\partial f_e}{\partial t} + \mathbf{v}_e \cdot \nabla_{\mathbf{x}} f_e + \frac{q_e}{m_e} \left(\mathbf{E} + \frac{\mathbf{v}_e}{c} \times \mathbf{B} \right) \cdot \nabla_{\mathbf{v}_e} f_e = \left(\frac{\partial f_e}{\partial t} \right)_i, \quad (2.1)$$

The right-hand side of equation (2.1) gives the change in f_e produced by encounters of electrons with ions and using Fokker-Planck equation it can be expressed as

$$\left(\frac{\partial f_e}{\partial t} \right)_i = C_{ee}(f_e, f_e) + C_{ei}(f_e, f_i). \quad (2.2)$$

In order to work with the right-hand side explicitly, we can write equation (2.2) using Taylor expansion (pages 94 to 96 in [19]) as

$$C_{ee}(f_e, f_e) + C_{ei}(f_e, f_i) = -\nu_{ei} \frac{\partial f \langle \Delta v_l \rangle}{\partial v_l} + \frac{\nu_{ei}}{2} \frac{\partial^2 f \langle \Delta v_l \Delta v_k \rangle}{\partial v_l \partial v_k}, \quad (2.3)$$

where ν_{ei} is the electron-ion collision frequency. Thus we get Vlasov-Fokker-Planck equation (VFP), that reads

$$\begin{aligned} \frac{\partial f_e}{\partial t} + \mathbf{v}_e \cdot \nabla_{\mathbf{x}} f_e + \frac{q_e}{m_e} \left(\mathbf{E} + \frac{\mathbf{v}_e}{c} \times \mathbf{B} \right) \cdot \nabla_{\mathbf{v}_e} f_e &= -\nu_{ei} \frac{\partial f \langle \Delta v_l \rangle}{\partial v_l} + \frac{\nu_{ei}}{2} \frac{\partial^2 f \langle \Delta v_l \Delta v_k \rangle}{\partial v_l \partial v_k}, \\ \langle \Delta v_l \rangle &:= \int \mathcal{P} \Delta v_l d^3(\Delta \mathbf{v}), \\ \langle \Delta v_l \Delta v_k \rangle &:= \int \mathcal{P} \Delta v_l \Delta v_k d^3(\Delta \mathbf{v}), \end{aligned} \quad (2.4)$$

where \mathcal{P} is transition function from state \mathbf{v} to $\mathbf{v} + \Delta \mathbf{v}$, complying normalization condition $\int \mathcal{P} d^3(\Delta \mathbf{v}) = 1$.

2.1 Kinetic models

Most kinetic models that describe particle transport in plasmas utilize VFP equations. One such model is the code called IMPACT [20], which was used to generate the data for our model described in the third chapter. IMPACT stands out as the first 2D VFP code to self-consistently include magnetic fields and it incorporates several other innovations. Firstly, it treats the electric field implicitly, along with the electron distribution function, which sets it apart from previous VFP codes. Secondly, it became the first 2D VFP code to solve the full matrix equation that arises when using implicit differencing. This fully implicit approach provides the benefit of making the code robust and capable of utilizing large time steps well beyond the characteristic collision time [20]. IMPACT employs VFP equation (2.4) in combination with Ampere's and Faraday's laws to describe the magnetic field. However, instead of directly dealing with VFP, IMPACT employs Cartesian tensor expansion

$$f_e(\mathbf{x}, \mathbf{v}, t) = \sum_p f_p(v, \mathbf{x}, t) :_p (\hat{\mathbf{v}})^p, \quad (2.5)$$

where $:_p$ represents tensor contraction over p indices. IMPACT employs the so-called diffusive approximation, which involves truncating the expansion at the first two terms. In other words, the distribution function $f_e(\mathbf{v}, x, y, z, t)$ is split into three parts: $f_e \approx f_0(v, x, y, t) + f_1(v, x, y, t) \cdot \hat{\mathbf{v}}$ with setting $f_z = 0$. The tensor expansion up to the first order is considered sufficient because the magnitudes of components of the Cartesian tensor series are ordered as $f_0 \sim \epsilon^{-1} f_1 \sim \epsilon^{-2} f_2$ etc., where $\epsilon = \lambda/L_n$, and $\lambda \ll \epsilon$ throughout. Nevertheless, the IMPACTA code was developed, which differs from IMPACT mainly by the inclusion of that second-order term f_2 [21]. Another new method based on IMPACT, that uses Finite Element Method was introduced in [22].

Instead of using tensor expansion it is also popular to approximate f_e with spherical harmonics as

$$f_e(\mathbf{x}, \mathbf{v}) = \sum_{l=0}^{N_l} \sum_{m=-N_m}^{N_m} f_l^m(\mathbf{x}, \nu, t) P_l^m(\cos \theta) e^{im\phi}, \quad (2.6)$$

where N_l, N_m are the number of terms in the expansion, and $P_l^m(\cos \theta)$ is the associated Legendre polynomial for the f_l^m term of the expansion. f_0^0 is the isotropic component of the distribution, while f_m^1 carries the first order vector information. Such expansion is used in OSHUN[23, 24] code, which is a successor of KALOS code, where the idea of different treatment of fast electrons (treated kinetically) and cold plasma (treated as a fluid) was used in order to economize computing resources.

As mentioned earlier, kinetic models offer the most accurate results, but this accuracy comes at the cost of significant computational expenses. To

reduce the time required for simulations, various hydrodynamic approaches have been proposed, and some of these approaches will be discussed in the next three sections.

2.2 Spitzer-Härm

The Spitzer-Härm (SH) approach first introduced in [25], also known as the Spitzer-Härm conductivity, is a widely used method for calculating heatflux in plasma. It provides an estimation of thermal conductivity by taking into account the interactions between charged particles and their surrounding medium.

Despite the result of SH we are interested in is the expression of heatflux as a hydrodynamic quantity, the derivation of Spitzer-Härm heatflux starts from Boltzmann's equation (2.1) and follows the same steps from (2.2) to (2.4). The approach is based on common assumptions such as neglecting all interactions between electrons for which the distance of closest approach (or collision parameter) exceeds the Debye length, and considering only collisions resulting in deflection of electrons at angles less than 90° . Besides these, the Spitzer-Härm approach is based on the following assumptions:

1. The Fokker-Planck equation may be used to give the collision term on the right-hand side of Equation (2.1).
2. A steady state is established.
3. The particle velocity is determined by the Maxwell velocity distribution f_0 with low perturbation f_1 , whose square may be neglected. Hence, $f = f_0 + f_1$.

The approximate electron distribution function satisfying the electron transport equation (2.4) takes the form [25]

$$f_e = \frac{n_e}{\left(\pi \frac{2k_B T_e}{m_e}\right)^{\frac{3}{2}}} \exp\left(-\frac{m_e |\mathbf{v}|^2}{2k_B T_e}\right) \left(1 - D\left(\frac{m_e |\mathbf{v}|^2}{2k_B T_e}\right)\right), \quad (2.7)$$

where the transport function reads

$$D(\omega) = \lambda(\omega - 4) \frac{\mathbf{n} \cdot \nabla_{\mathbf{x}} T_e}{T_e}, \quad (2.8)$$

In paper [26] the function $D(\omega)$ was further extended by the electron-electron collision operator, which had to be solved numerically. The latter concludes, that the mean free path of electrons should be adjusted as

$$\lambda_{\text{SH}} = \frac{0.024Z + 0.058}{1 + 0.24Z} \lambda. \quad (2.9)$$

After integrating the equation (2.7) over the velocity space, one obtains[12]:

$$q = -\kappa_{\text{SH}} T^{\frac{5}{2}} \nabla T, \quad (2.10)$$

where κ_{SH} is

$$\kappa_{\text{SH}} = \frac{(Z + 0.24)}{(Z + 4.2)} \frac{1.31 \times 10^{10}}{Z \Lambda_{ei}} \quad (2.11)$$

and the Coulomb logarithm is (see NRL Plasma Formulary [27])

$$\Lambda_{ei} = 23 - \ln \left(\frac{\sqrt{n_e} Z}{T_e^{3/2}} \right).$$

The Spitzer-Härm approach provides a reasonable approximation of the heatflux in many plasma scenarios, including laboratory experiments and astrophysical plasmas. However, it has limitations and may not accurately capture the behavior of highly non-equilibrium or strongly magnetized plasmas. In such cases, more sophisticated models or numerical simulations are required.

Thanks to its relative simplicity, the Spitzer-Härm approach has significantly contributed to the understanding of heat transport in plasmas. It has been and still is extensively applied in various fields, including fusion research, astrophysics, and space physics, enabling researchers to analyze and predict the behavior of plasma systems under different conditions. However, as we will show later, the Spitzer-Härm approach has its limitations, especially in cases where nonlocal electron transport is present, since the Spitzer-Härm solution for heatflux is still dependent only on local plasma parameters.

2.3 Heatflux limiter

In the hotter region of the heat front, the heatflux is observed to be several times smaller than the value given by the SH description, and is limited to a fraction $\approx 0.1 - 0.2$ of the free-streaming value $q_{\text{fs}} = v_{\text{th}} n_e k_B T$, where $v_{\text{th}} = \sqrt{k_B T_e / m_e}$.

On the contrary, at the base of the heat front, the conductivity exceeds the SH conductivity, because the flux has a nonlocal part due to the hot, nearly collisionless electrons streaming away from the top of the heat front. Fluid codes describing laser-irradiated targets usually model the heatflux by a local law of the type $q = \min(q_{\text{SH}}, f_{\text{lim}} q_{\text{fs}})$, where q_{SH} , is the SH heatflux (2.10), and f_{lim} is the flux-limit factor.

From the definition of Knudsen number Kn it is seen that nonlocal transport lies somewhere between diffusive transport and free streaming of particles. Heatflux limiter approach combines both modes of transport and evaluates it as a continuous transition from q_{SH} to q_{fs} . One of the possible definitions of

limited heatflux reads:

$$q_{\text{lim}} = f_{\text{lim}} q_{\text{fs}} \left(1 - \exp \left(\frac{-q_{\text{SH}}}{f_{\text{lim}} q_{\text{fs}}} \right) \right), \quad (2.12)$$

where f_{lim} is the already mentioned flux-limit factor varying between 0.03 and 0.15.

2.4 Convolution LMV and SNB models

However, as was pointed out and as we will show later, the description of heatflux in (2.12) is deficient in modeling heat transport in many respects, and it cannot take into account its nonlocal character. Hence a new approach was introduced in paper of Luciani Mora and Virmont (LMV) [28].

The LMV approach aims to estimate the heatflux and energy transport in ICF implosions with improving the Spitzer-Härm heatflux (2.10). LMV is not dependent only on local plasma parameters, it considers the parameters all along the profile by applying the convolutional kernel

$$q_{\text{SNB}} = \int_{-\infty}^{\infty} W(\mathbf{x}, \mathbf{x}') q_{\text{SH}}(\mathbf{x}') \frac{d\mathbf{x}'}{a \lambda_e(\mathbf{x}')}, \quad (2.13)$$

where a is an adjustable parameter, according to [28] $a \in (30, 35)$, λ_e is an effective collision mean free path given by

$$\lambda_e = (Z + 1)^{-1/2} \frac{(k_B T_e)^2}{4\pi n_e e^4 \log \Lambda} \quad (2.14)$$

and the convolution kernel reads

$$W(\mathbf{x}, \mathbf{x}') = \frac{1}{2a(Z + 1)^{1/2} \lambda_e(\mathbf{x}')} \exp \left(- \left| \frac{\int_{\mathbf{x}'}^{\mathbf{x}} n_e \mathbf{x}'' d\mathbf{x}''}{a(Z + 1)^{1/2} \lambda_e(\mathbf{x}') n_e(\mathbf{x}')} \right| \right). \quad (2.15)$$

In the original paper of Luciani et al. the term $W(\mathbf{x}, \mathbf{x}')$ behaves like a δ function, so for small temperature and density gradients the heatflux given by (2.13) behaves exactly like heatflux provided by Spitzer and Härm from (2.10).

The original 1D LMV model was further extended into higher dimensions by Schurtz, Nikolai and Busquet (SNB)[18]. But we will not further describe it here, since just like LMV we will consider one-dimensional profiles of plasma parameters.



Chapter 3

Machine Learning-Driven Hydrodynamic Closure

The creation of our model was motivated by the need for a relatively quick calculation of heatflux that would correspond to nonlocal transport. For this reason a deep learning forward Multilayer Perception (MLP) consisting of two hidden layers was implemented using PyTorch Lightning[29] library in Python programming language.

Here I would like to mention once again a work of Lamy et. al. where ANN predicting heatflux was used to replace SNB module [8]. Similar to our approach, they implemented the ANN in Python. But unlike our work, the neural network replaced the hydrodynamic model, not the kinetic one, however, their work was also carried out in 2D.

Neural networks are an example of nonlinear operators consisting of a hierarchy of layers, where weights and parameters of the activations functions are adjusted (trained). An example of a modern architecture suitable for our regression problem that includes adaptive activation functions is reviewed in [30]. Physics-informed neural networks (PINNs) represent another class focusing on inherent physical mechanisms encrypted by using PDE as a part of the loss function. PINNs are considered state-of-the-art PDE solvers requiring minimal data input [31]. Next, convolution neural networks (CNNs) have been successfully used for regression problems in multiple dimensions like the ones we would need to solve for radiation hydrodynamic closure [32]. The model above also uses transfer learning [33, 34, 35, 36]. By means of a recurrent neural network (RNN) development known as “long short-term memory”, which allows the model to retrain useful dependencies and adapt the accuracy to new datapoints [37]. Lastly, Transformers represent a very robust and successful architecture to surrogate operators. In particular, the Vision Transformer (ViT)[38, 39], they would be an excellent model for more complex models beyond the heat flux moment of the distribution function. However, in order to get competitive performance out of a transformer, one needs to train it on a significantly more data than a traditional neural network.

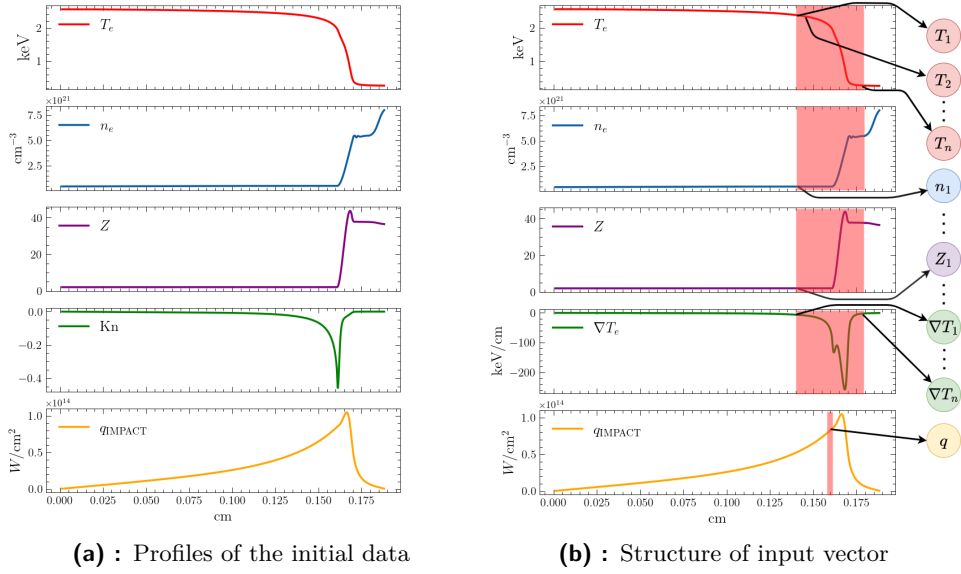


Figure 3.1: Profiles of the initial data and construction of data vector. Each profile contains 400 datapoints.

The training of our MLP took place using ReLU[40] activation function, and Mean Squared Error (MSE) as a loss function. The latter was minimized with the Stochastic gradient descent (SGD)[41] optimizer.

In order to describe our model in more detail we will start with introducing the initial data, on which the MLP was trained, tested and using which MLP was compared with other models mentioned previously.

3.1 Data preparation

The initial data represents five profiles of different plasma parameters: electron temperature T_e , heatflux q_{IMPACT} , electron density n_e , relative ionization rate Z and Knudsen number Kn . The latter wasn't eventually used in our MLP but the profile of Kn is still representative in terms of spatial localization of nonlocal transport, moreover calculated Kn was later used to correct the conduction parameter α given by MLP in time evolution of the temperature profile. The calculation of q_{IMPACT} was performed using the IMPACT code. The data generated by IMPACT [42] represents the values of the plasma parameters at 20 ns after a simulated laser heats the wall of hohlraum (placed on the right side of the profile, where n_e reaches its highest values). These profiles are shown in Fig. 3.1a. Data used for training and validation of our MLP was prepared by partitioning 400 point long initial profiles into segments, each consisting of 23 consecutive spatial points, over a $476 \mu\text{m}$ interval, containing 23 points. We collected data for the following plasma parameters: electron temperature T_e , electron density n_e , ionization rate

Z , gradient of electron temperature ∇T_e , and the single value of heatflux q_{IMPACT} sitting at the center of the interval. The composition of 23×4 values of T_e , n_e , ∇T_e , Z appertaining to 23 spatial points will be called *input vector*, and the value of heatflux appertaining to the center of that interval will be used for training of the MLP. Figure 3.1b depicts the construction of one such input vector with q included.

The rationale behind this approach is that the heatflux at any spatial point depends not only on the values of the plasma parameters at that point but also on the values of these parameters in the surrounding region. This way we incorporate nonlocality into our model.

The same operation then was performed over all intervals of the same length along the x -axis in a manner similar to a convolutional process, thus creating a dataset used for training and testing the MLP.

3.2 Multilayer perceptron

The basic component of MLP is the neuron, representing a single number and connected to every other neuron of adjacent layers. It takes an input of N dimensions, multiplies it by a weight matrix, adds a nonlinear variable called bias, and passes the result in the activation function, which in our case is the ReLU function $f_{\text{ReLU}}(x) = \max\{0, x\}$. Mathematically, the calculation of j -th neuron belonging to $l+1$ -st layer reads[8]

$$a_j^{l+1} = f_{\text{ReLU}} \left(\sum_{i=1}^N a_i^l w_{i,j}^{l+1} + b_j^{l+1} \right), \quad (3.1)$$

where l is a layer's index. Our MLP consists of the input layer \vec{V} , two hidden layers \vec{L}_1 and \vec{L}_2 , and output layer \vec{R} . Those layers are connected by weight matrices $w_{ij}^{1,2,3}$ and biases $\vec{b}^{1,2,3}$. Each i -th neuron of the input layer \vec{V} is equal to the i -th component of input vector we defined in previous section, consequently their lengths are also equal. We have set the lengths of both hidden layers \vec{L}_1 and \vec{L}_2 equal to 30. Finally the output layer consists of 2 neurons, one for the heatflux and one for conduction parameter β . The representative scheme of our MLP is shown in the Fig. 3.2.

All the neurons and biases of the MLP are adjustable (trainable) and during the training they are adjusted so that, the difference between the result of MLP action and the values we recognize as accurate (training data) is as small as possible. In order to achieve this we use the method called Stochastic Gradient Descent (SGD). The method resides in representing the Mean Squared Error (MSE) of the values of output layer neurons \vec{R} w.r.t. training data \vec{Y} as a function of all the neurons and biases,

$$\text{MSE} = \frac{1}{n} \sum_i (R_i - Y_i)^2 = \text{MSE} \left(w_{ij}^{1,2,3}, \vec{b}^{1,2,3} \right). \quad (3.2)$$

In order that MLP gives a precise result we want to minimize MSE, which is achieved by calculating the gradient of MSE and iteratively changing the neurons, weights and biases in direction of the descending gradient. Mathematically, if we label all the variables of MSE as \mathbf{x} then one change of \mathbf{x} according to SGD can be written as

$$\mathbf{x} := \mathbf{x} - \eta \nabla \text{MSE}(\mathbf{x}), \quad (3.3)$$

where η is a constant often called learning rate, and the change of \mathbf{x} described by equation (3.3) is called learning step. The distinguishing feature of SGD method is that one learning step is made for only one sample of training data chosen randomly from the whole training database.

We have trained our MLP on 40% of the whole database prepared by the convolutional process, described earlier. 10% of the database was dedicated to validation, and the remaining 50% for testing of the MLP. All three sets of data were picked randomly and exclusively from the database.

As a result the MLP prediction of the q heat flux is depicted in Fig. 3.3. While externally the curve predicted by the MLP aligns with the kinetic simulation data, the issue arises from the oscillating behavior of the gradient ∇q , as is evident in the graph shown in Fig. 3.4. These oscillations will pose a significant problem when dealing with the time evolution of the temperature profile, given that ∇q is a key component in the equation of heat conduction.

A comparison of heat flux profiles calculated using different models is presented in Figure 3.5. From this figure, it is evident that our trained model provides results closest to those of the kinetic model on which the model was trained. This outcome is expected, and it is worth noting that for a more unbiased assessment of the model's effectiveness, a larger amount of data would be required both for training and comparison. Since we do not possess additional data for training, we can at least compare the behavior of the models when simulating the time evolution of the temperature profile. The next section is mainly dedicated to the implementation of our MLP model to solve the thermal transport problem.

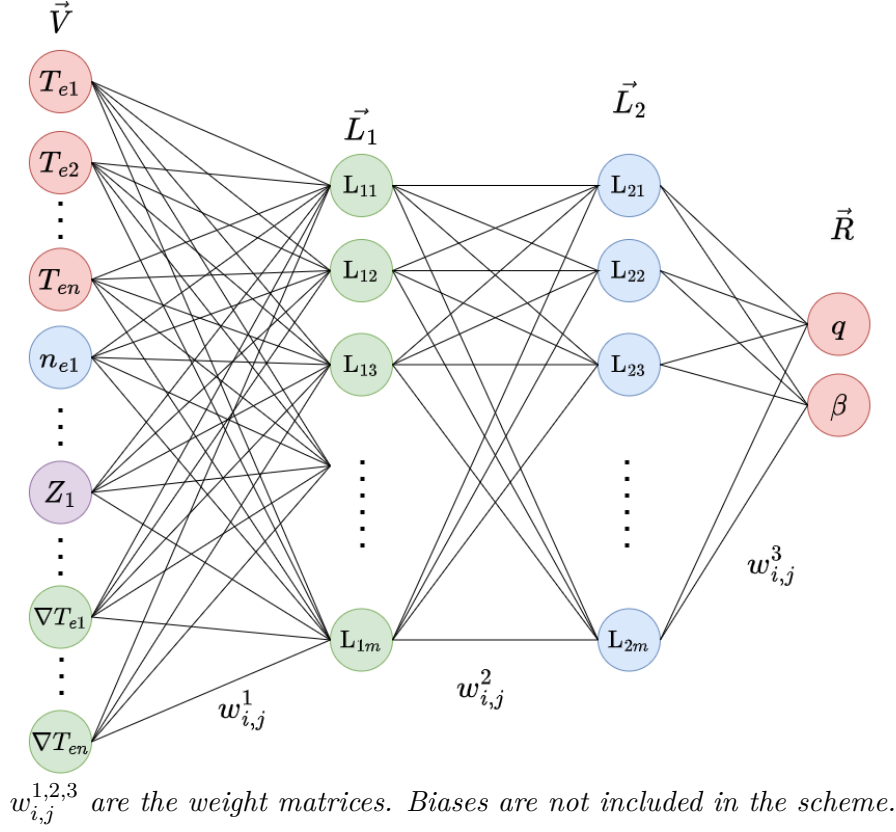


Figure 3.2: The representative scheme of MLP structure.

3.3 Novel nonlocal thermal transport model

We want to solve the **heat conduction** model

$$\frac{d\varepsilon(t, x)}{dt} = -\nabla \cdot \mathbf{q}(t, x), \quad (3.4)$$

where

$$\mathbf{q}(t, x) = -\alpha(t, x)\kappa(t, x)T(t, x)^{\beta(t, x)}\nabla T(t, x), \quad (3.5)$$

and

$$\varepsilon(t, x) = C_V(x)T(t, x) = \frac{3}{2}n(x)k_B T(t, x), \quad (3.6)$$

and $\alpha(t, x)$ is a **MLP-driven** variable heat flux limiter and $\beta(t, x)$ is obtained as a fit to self-similar solution with nonlinearity n of the heat wave from planar source given by Eq. 10.32, Section X.5 in [43], see Figure 3.6.

The variables are written in Gauss units $\varepsilon \left[\frac{\text{erg}}{\text{cm}^3} \right]$, $T[\text{eV}]$, $q \left[\frac{\text{erg}}{\text{cm}^2} \right]$ with $k_B = 1.380649 \times 10^{-16} \frac{\text{erg}}{\text{K}} = 1.602178 \times 10^{-12} \frac{\text{erg}}{\text{eV}}$ and α, β are dimensionless.

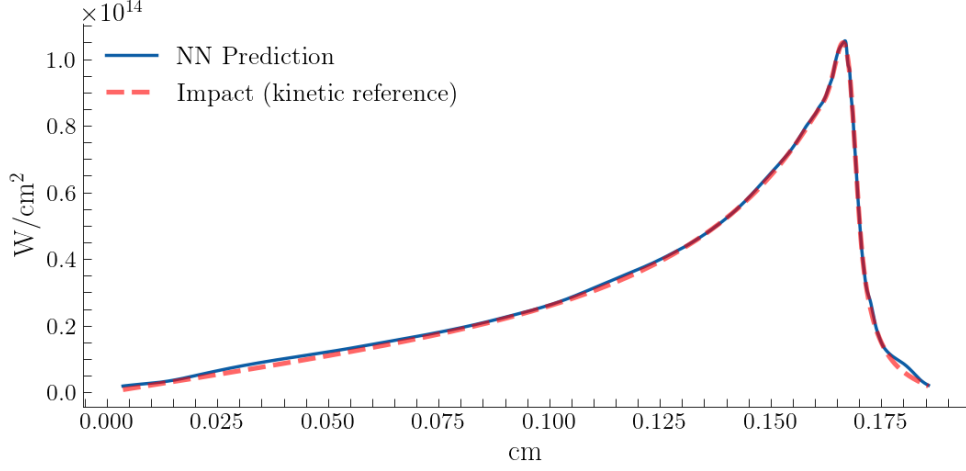


Figure 3.3: Profile of neural network prediction compared to kinetic reference IMPACT.

The conductivity κ in our model is defined in Gauss units as

$$\kappa(t, x) = \kappa_{\text{SH}} \tau^{\beta(t, x) - \frac{5}{2}}, \quad (3.7)$$

where κ_{SH} is Spitzer-Härm conductivity from (2.11) and $\tau = \frac{1}{T_{\text{preheat}}}$.

The electron of velocity v travels the mean free path in background plasma at density n_e , temperature T_e , and ionization Z (electron-electron and electron-ion combined effect approximated by Epperlein [44])

$$\lambda(v, n_e, Z, T_e) = \frac{v^4}{n_e \Gamma \Lambda_{ei}(n_e, Z, T_e)} \frac{1}{\sqrt{Z+1}}, \quad (3.8)$$

where $\Gamma = \frac{4\pi q_e^4}{m_e^2} = 8.06 \times 10^{17}$ in Gauss units. Commonly, the mean free path refers to the mean free path of thermal electron

$$\lambda_{th} = \lambda(v = \sqrt{k_B T_e / m_e}, n_e, Z, T_e). \quad (3.9)$$

Knudsen number $\text{Kn} = \frac{\lambda_{th}}{L}$, where $L = \frac{T_e}{|\nabla T_e|}$ is the characteristic electron distribution scale length, represents a non-dimensional parameter characterizing the local transport regime if $\text{Kn} < 10^{-3}$.¹

We use $T_{\text{preheat}} = 2.5$ keV to safely include the preheat region of the hohlraum wall simulation.

Inhibition ratio $R_q = \frac{q_{\text{SH}}}{q_{\text{MLP}}}$, where q_{SH} is Spitzer-Härm heatflux (2.10), can be evaluated at every point of the neighborhood and post-processed through convolution to obtain a nonlocal information \bar{R}_q . We expect $\beta \xrightarrow{\bar{R}_q \gg 1} 2.5$ and $\beta \xrightarrow{\bar{R}_q \ll 1} 0$.

¹In case that $\text{Kn} < 10^{-3}$ we can express α as $\alpha = 1 + \text{Kn} + O(\text{Kn}^2)$. This happens in local diffusion approximation in (3.5) and $\beta = 2.5$.

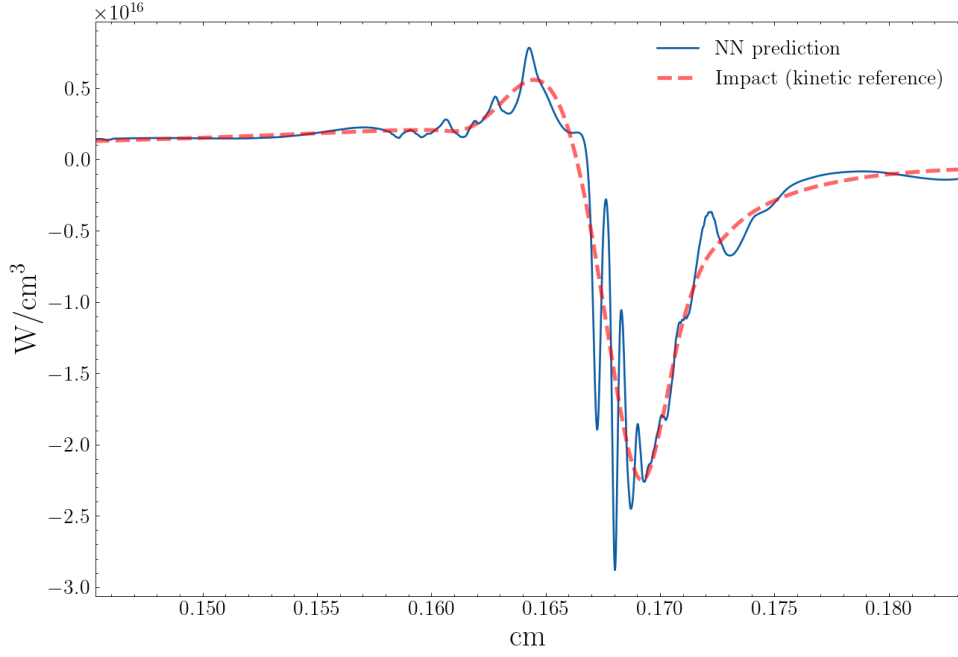


Figure 3.4: ∇q profile of neural network prediction compared to kinetic reference IMPACT.

Practically both $\alpha(t, x)$ and $\beta(t, x)$ are given by MLP ², but α is calculated indirectly from heatflux q_{MLP} as inverted inhibition ratio R_q^{-1}

$$\alpha = \frac{q_{\text{MLP}}}{q_{\text{SH}}}. \quad (3.10)$$

This definition raises a problem at the edges of the profile, where q_{SH} is effectively zero. Thus we define and use a corrected value α_{cor} as

$$\alpha_{\text{cor}} = 1 + \frac{s(\alpha - 1)\text{Kn}^2}{1 + s\text{Kn}^2}, \quad (3.11)$$

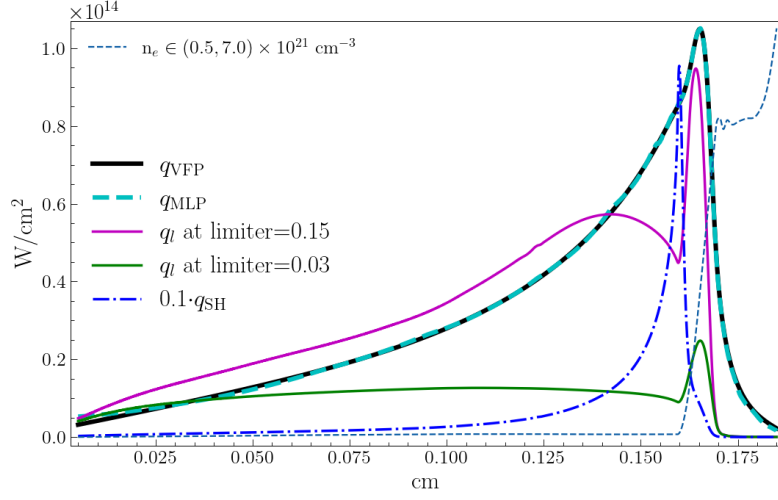
where parameter s was empirically set equal to 2.5×10^5 . The motivation behind this definition is that $\alpha_{\text{cor}} \xrightarrow{\text{Kn} \ll 1} 1$ and $\alpha_{\text{cor}} \xrightarrow{\text{Kn} \sim 1} \alpha$. This eliminates the problem of α rising effectively to infinity at edges of the profile. From this point on, we will keep α_{cor} in mind when mentioning α , thus $\alpha := \alpha_{\text{cor}}$

In order to solve (3.4), (3.5), and (3.6), we define a functional in 1D

$$F(T) := C_V \frac{dT}{dt} - \frac{d}{dx} \underbrace{\left(\alpha(T) \kappa T^{\beta(T)} \frac{dT}{dx} \right)}_q \quad (3.12)$$

and our task will be to find T that solves

$$F(T) = 0. \quad (3.13)$$



q_{VFP} heat flux profile provided by IMPACT[42]. q_l is a heatflux predicted by heatflux limiter (2.12)

Figure 3.5: Nonlocal heat flux within the expanding hohlraum wall

We discretize the problem on a general 1D mesh with cell-related variables indexed by integers and node-related ones by half-integers, as shown in Fig. 3.7.

Thus the cell volume is

$$\Delta x_i = x_{i+\frac{1}{2}} - x_{i-\frac{1}{2}}, \quad (3.14)$$

while the volume of the node-assigned dual cell (distance between neighboring cell centers) is

$$\Delta x_{i+\frac{1}{2}} = x_{i+1} - x_i = \frac{\Delta x_i + \Delta x_{i+1}}{2}. \quad (3.15)$$

The divergence of q in (3.4) is discretized on the primary cell by the finite difference

$$\nabla \cdot \mathbf{q}|_i \stackrel{1D}{=} \frac{dq}{dx}|_i \approx \frac{q_{i+\frac{1}{2}} - q_{i-\frac{1}{2}}}{\Delta x_i}, \quad (3.16)$$

with the nodal value of the flux (3.5) being approximated as

$$q_{i+\frac{1}{2}} = \overline{(\alpha\kappa T^\beta)}_{i+\frac{1}{2}} \frac{T_{i+1} - T_i}{\Delta x_{i+\frac{1}{2}}}, \quad (3.17)$$

where $\overline{(\alpha\kappa T^\beta)}_{i+\frac{1}{2}}$ is obtained by some kind of averaging from the two

²MLP was trained to return values of heatflux close to results of kinetic simulation, but moreover MLP also returns values of β close to the β from self-similar solution.

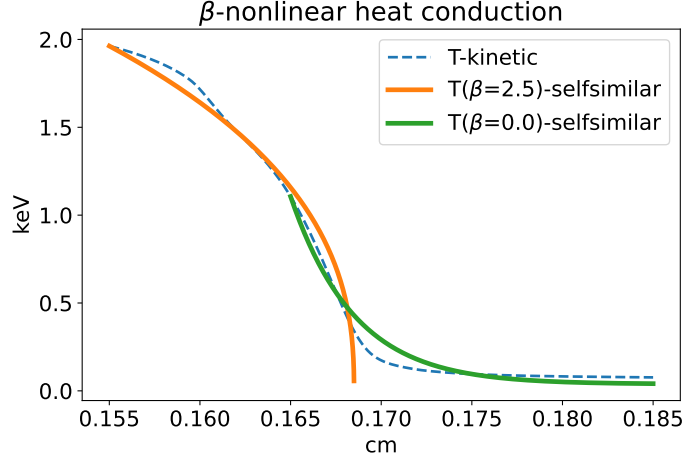


Figure 3.6: Self-similar "conductive nonlinearity" exhibited by preheat.

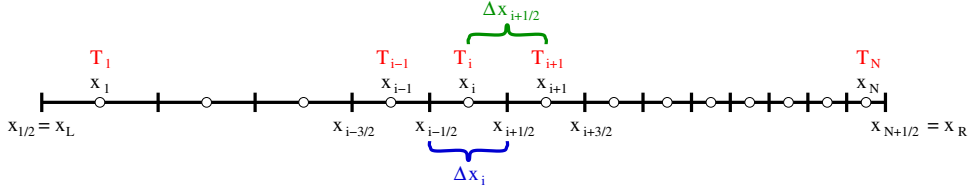


Figure 3.7: Discretization of the 1D problem

connected cells, for example

$$\overline{(\alpha\kappa T^\beta)}_{i+\frac{1}{2}} = \frac{(\alpha\kappa T^\beta)_i + (\alpha\kappa T^\beta)_{i+1}}{2}, \quad (3.18a)$$

$$\overline{(\alpha\kappa T^\beta)}_{i+\frac{1}{2}} = \frac{\Delta x_i (\alpha\kappa T^\beta)_i + \Delta x_{i+1} (\alpha\kappa T^\beta)_{i+1}}{\Delta x_i + \Delta x_{i+1}}, \quad \text{or} \quad (3.18b)$$

$$\overline{(\alpha\kappa T^\beta)}_{i+\frac{1}{2}} = \frac{\frac{1}{\Delta x_i} (\alpha\kappa T^\beta)_i + \frac{1}{\Delta x_{i+1}} (\alpha\kappa T^\beta)_{i+1}}{\frac{1}{\Delta x_i} + \frac{1}{\Delta x_{i+1}}}, \quad (3.18c)$$

where we denoted

$$(\alpha\kappa T^\beta)_j = \alpha_j \kappa_j T_j^{\beta_j}. \quad (3.19)$$

Discretizing (3.13), resp. (3.4), (3.5), and (3.6) over the i -th cell, we have

$$F_i := C_V i \frac{dT_i}{dt} - \frac{\overline{(\alpha\kappa T^\beta)}_{i+\frac{1}{2}} \frac{T_{i+1} - T_i}{\Delta x_{i+\frac{1}{2}}} - \overline{(\alpha\kappa T^\beta)}_{i-\frac{1}{2}} \frac{T_i - T_{i-1}}{\Delta x_{i-\frac{1}{2}}}}{\Delta x_i} \quad (3.20)$$

with space-dependent α and β being provided by the neural network and k , C_V being also functions of x :

$$\alpha = \alpha(\text{NN}(x), \text{Kn}(x)), \quad \beta = \beta(\text{NN}(x)), \quad k = k(Z(x)), \quad C_V = C_V(n(x)). \quad (3.21)$$

At this point let us remark, that classical heat conductivity in plasma uses constant $\beta = 5/2$, which further simplifies the equations. This is the case for example in [45]. However, there the problem is transformed using $\theta = T^{7/2}$ and solved by a mimetic scheme, whereas here we are going to proceed by Newton's iterative method.

For a regular mesh (i.e., with equidistant nodes), we have

$$\Delta x = \Delta x_i = \Delta x_{i+\frac{1}{2}}, \quad \forall i, \quad (3.22)$$

and thus (3.20) simplifies to

$$F_i = C_{V_i} \frac{dT_i}{dt} - \frac{1}{\Delta x^2} \left(\overline{(\alpha\kappa T^\beta)}_{i+\frac{1}{2}} (T_{i+1} - T_i) - \overline{(\alpha\kappa T^\beta)}_{i-\frac{1}{2}} (T_i - T_{i-1}) \right) \quad (3.23)$$

and all three types of averaging (3.18) are equivalent:

$$\overline{(\alpha\kappa T^\beta)}_{i+\frac{1}{2}} = \frac{(\alpha\kappa T^\beta)_i + (\alpha\kappa T^\beta)_{i+1}}{2}. \quad (3.24)$$

There are several ways to solve (3.13), that is, in the discrete case

$$F_i(\mathbf{T}) = 0, \quad \forall i. \quad (3.25)$$

Replacing also the time derivative by a finite difference, (3.23) becomes

$$F_i(\mathbf{T}) = C_{V_i} \frac{T_i - T_i^{[t-\Delta t]}}{\Delta t} - \frac{1}{\Delta x^2} \left(\overline{(\alpha\kappa T^\beta)}_{i+\frac{1}{2}} (T_{i+1} - T_i) - \overline{(\alpha\kappa T^\beta)}_{i-\frac{1}{2}} (T_i - T_{i-1}) \right), \quad (3.26)$$

where $T_i^{[t-\Delta t]}$ is the temperature at the previous time level $t - \Delta t$. Note that by using temperature at the actual time level t in the spatial difference (the term in parentheses), we are aiming at implicit schemes, so that the time step Δt is not overrestricted by stability requirements.

3.3.1 Newton's iteration

For simplicity, let us take in each equation the value of $(\alpha\kappa T^\beta)$ from the actual cell instead of using nodal averages at its endpoints. Then we have a system similar to (3.25) with the i -th equation being

$$F_i^*(\mathbf{T}) = C_{V_i} \frac{T_i - T_i^{[t-\Delta t]}}{\Delta t} - \alpha_i \kappa_i T_i^{\beta_i} \frac{T_{i-1} - 2T_i + T_{i+1}}{\Delta x^2}. \quad (3.27)$$

The Jacobian of such system is a tridiagonal matrix with the elements

$$J_{i,i} = \frac{\partial F_i^*}{\partial T_i} = \frac{C_{Vi}}{\Delta t} + 2 \frac{\alpha_i k_i}{\Delta x^2} (\beta_i + 1) T_i^{\beta_i} \quad (3.28a)$$

$$J_{i,i\pm 1} = \frac{\partial F_i^*}{\partial T_{i\pm 1}} = - \frac{\alpha_i k_i T_i^{\beta_i}}{\Delta x^2}. \quad (3.28b)$$

Using the exact definition of nonlinear functional F given by (3.26) and approximate Jacobian (3.28), we can now perform the k -th iteration of Newton's method:

$$\mathbf{T}^{(k+1)} = \mathbf{T}^{(k)} - \mathbf{J}^{-1} \mathbf{F}(\mathbf{T}^{(k)}). \quad (3.29)$$

Keep in mind, that the superscript (k) stands for Newton's iteration, not for the evolution in time! Therefore, $T_i^{[t-\Delta t]}$ in (3.27) stays the same in all iterations at given time t , until the solution \mathbf{T} at this time level has converged.

If we require an exact Jacobian, we can obtain it by deriving from the equation (3.26) using (3.18). Consequently, it can be deduced that:

$$J_{i,i} = \frac{\partial F_i}{\partial T_i} = \frac{C_{Vi}}{\Delta t} + \frac{1}{\Delta x^2} \left(\frac{1}{2} \alpha_{i+1} k_{i+1} T_{i+1}^{\beta_{i+1}} + \frac{1}{2} \alpha_{i-1} k_{i-1} T_{i-1}^{\beta_{i-1}} + \right. \quad (3.30a)$$

$$\left. + (\beta_i + 1) \alpha_i k_i T_i^{\beta_i} - \frac{1}{2} \beta_i \alpha_i k_i T_i^{\beta_i-1} (T_{i+1} + T_{i-1}) \right)$$

$$J_{i,i\pm 1} = \frac{\partial F_i}{\partial T_{i\pm 1}} = \frac{1}{\Delta x^2} \left(\frac{1}{2} \beta_{i\pm 1} \alpha_{i\pm 1} k_{i\pm 1} T_{i\pm 1}^{\beta_{i\pm 1}-1} T_i - \right. \quad (3.30b)$$

$$\left. - \frac{1}{2} (\beta_{i\pm 1} + 1) \alpha_{i\pm 1} k_{i\pm 1} T_{i\pm 1}^{\beta_{i\pm 1}} - \frac{1}{2} \alpha_i k_i T_i^{\beta_i} \right)$$

3.3.2 Boundary conditions

We will enforce

$$\nabla T = 0 \quad (3.31)$$

on both ends of the domain. To do this on a mesh of N cells indexed from 1 to N (see Fig. 3.7), we formally introduce the ghost values

$$T_0 = T_1, \quad T_{N+1} = T_N. \quad (3.32)$$

Inserting them into the equations (3.27) for the boundary cells ($i = 1$ resp. $i = N$), we get

$$F_1(\mathbf{T}) := C_{V1} \frac{T_1 - T_1^{[t-\Delta t]}}{\Delta t} - \frac{(\overline{\alpha \kappa T^\beta})_{\frac{3}{2}} (T_2 - T_1)}{\Delta x^2}, \quad (3.33a)$$

$$F_N(\mathbf{T}) := C_{VN} \frac{T_N - T_N^{[t-\Delta t]}}{\Delta t} + \frac{(\overline{\alpha \kappa T^\beta})_{N-\frac{1}{2}} (T_N - T_{N-1})}{\Delta x^2}, \quad (3.33b)$$

which immediately yields the first and last row of the Jacobian matrix

$$J_{1,1} = \frac{\partial F_1^*}{\partial T_1} = \frac{C_{V1}}{\Delta t} + \frac{\alpha_1 \kappa_1}{\Delta x^2} (\beta_1 + 1) T_1^{\beta_1}, \quad (3.34a)$$

$$J_{1,2} = \frac{\partial F_1^*}{\partial T_2} = -\frac{\alpha_1 \kappa_1 T_1^{\beta_1}}{\Delta x^2}, \quad (3.34b)$$

$$J_{N,N-1} = \frac{\partial F_N^*}{\partial T_{N-1}} = -\frac{\alpha_N \kappa_N T_N^{\beta_N}}{\Delta x^2}, \quad (3.34c)$$

$$J_{N,N} = \frac{\partial F_N^*}{\partial T_N} = \frac{C_{VN}}{\Delta t} + \frac{\alpha_N \kappa_N}{\Delta x^2} (\beta_N + 1) T_N^{\beta_N}. \quad (3.34d)$$

Chapter 4

Results

We have implemented the implicit Newton solver of the equation (3.13) and set the convergence condition as a condition on a relative difference between mean energies

$$\frac{\overline{E}^{[t-\Delta t]} - \overline{E}^{[t]}}{\overline{E}^{[t-\Delta t]}} \leq 10^{-9}, \quad (4.1)$$

where \overline{E} is calculated as

$$\overline{E} = \frac{\frac{3}{2}k_B \sum_i^N n_i T_i}{N}. \quad (4.2)$$

After making roughly 300-400 time steps, corresponding to 0.4 ns for every model, we obtained the results shown in Figures 4.1, 4.2 and 4.3 corresponding to MLP, SH and heatflux limiter model respectively. It is rather clear from the definition of the convergence condition (4.1) that for every simulation run the energy losses don't exceed $(4 \times 10^{-7})\overline{E}_0$, where \overline{E}_0 is the initial value of the mean energy of the profile.

The difference between the solutions is rather evident in Fig. 4.4. This graph compares profiles of T at time 0.4 ns that were obtained with the all three models used in our simulation. From the this graph it is already clear, that during the time evolution of T our MLP model exhibits the suppression of α in the region of high density and temperature gradients just like heatflux limiter model does, though MLP also shows results of preheat, absence of which is the heatflux limiter's weakness.

These conclusions can be made just by the course of temperature profiles, but we also have tried to show it directly in Fig. 4.5, where the time evolution of α is shown using color. α is smallest in the region of highest value of Kn both for MLP and heatflux limiter, while α_{MLP} has additional peaks where α_{MLP} exceeds 1 around the pit, whereas α_{lim} remains smaller than 1 everywhere.

In Fig. 4.5, it is also visible that α_{MLP} exceeds 1 not only in regions where preheat is expected but also in the left half of the profile where

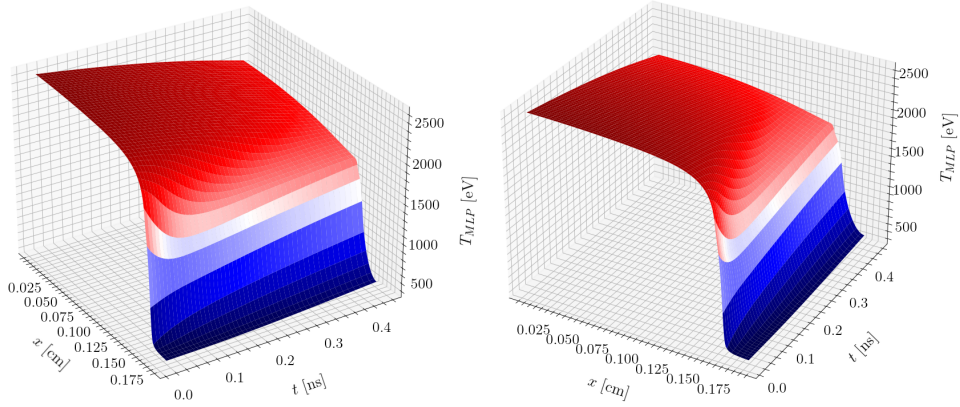


Figure 4.1: Time evolution of T according to MLP solver

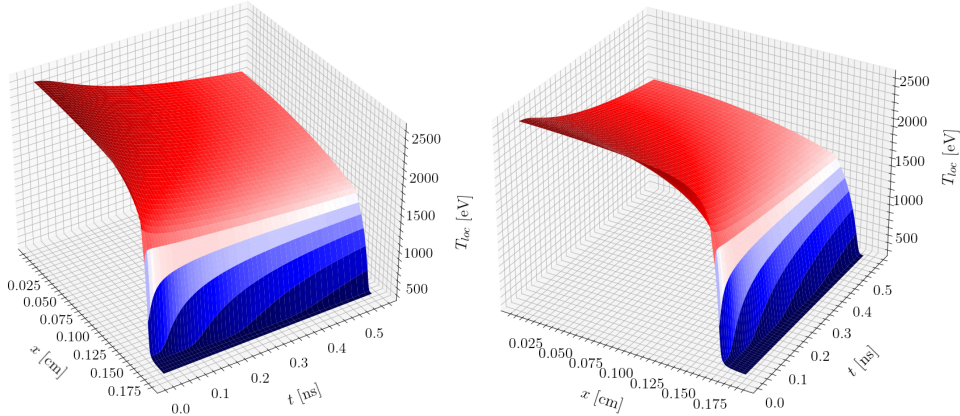


Figure 4.2: Time evolution of T according to SH heatflux (2.10)

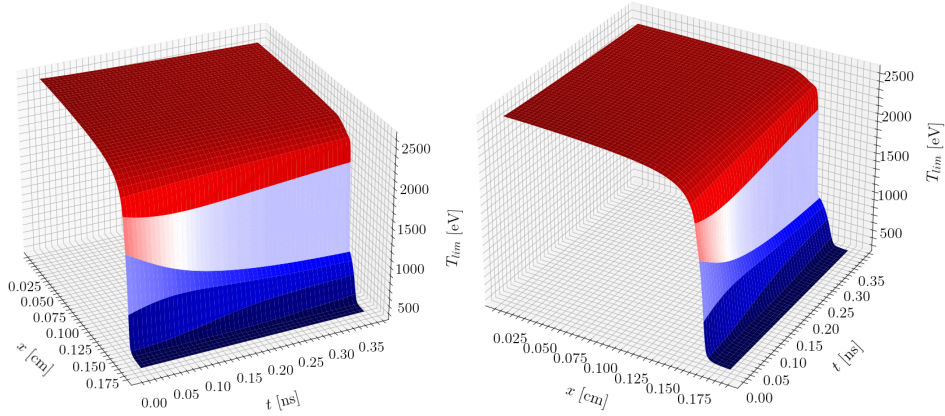


Figure 4.3: Time evolution of T according to heatflux limiter (2.12)

$\text{Kn} \ll 1$, indicating the diffusive mode of transport. This behavior is a result of MLP returning a heat flux well exceeding zero in the region of nearly zero temperature gradient (see Fig. 4.8). Such unexpected behavior can be considered as an inaccuracy of MLP induced by the supposed lack of training

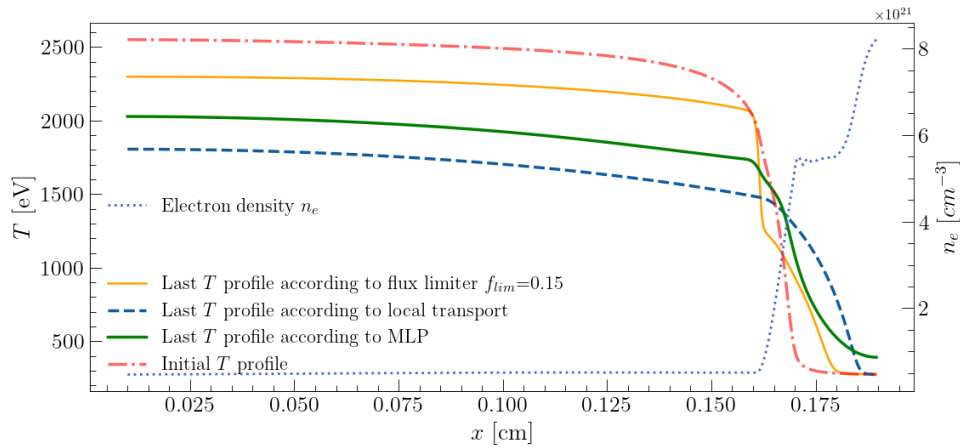


Figure 4.4: Comparison of the final profiles ($t=0.4$ ns) of the solutions.

on various shapes of temperature profiles.

This lack of training also manifests itself in that every newly trained MLP produces results that follow the same trend although differ from each other. For instance, in Fig. 4.6, the last temperature profiles obtained from different MLPs are compared with each other. Although all the profiles have the same course, there's deviation along the whole x -axis with some outlying results. This leads to the need of rechecking of the trained MLP before the simulation run. A graph of the mean profile of 70 different simulations results with standard deviation is depicted in Fig. 4.7. From that figure we see that relative deviation reaches 6.6% of the mean profile given by MLPs exactly in the region of the highest interest, where the highest temperature and density gradients are present.

These deviations are caused by randomized process of the training on relatively small amount of data, residing first in SGD training process and second in random selection of the training, validation and testing sets for each individual MLP. This comparison is depicted in Fig. 4.7. This comparison shows positively the consistency of different MLPs, but does not say anything about the accuracy of the model itself. It is still possible that all the results given by the network are beyond a reasonable deviation from the results that would show kinetic simulations. Being a significantly faster method compared to kinetic models (10^6 computationally less expensive [46]), our MLP model, of course, does not claim the same accuracy that is given by kinetic models.

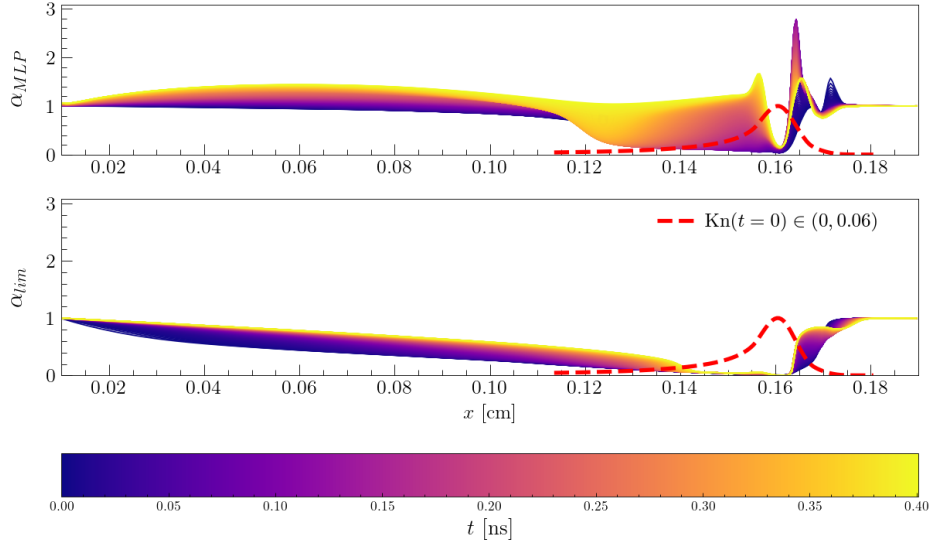


Figure 4.5: Comparison of coefficients α given by MLP and heatflux limiter respectively

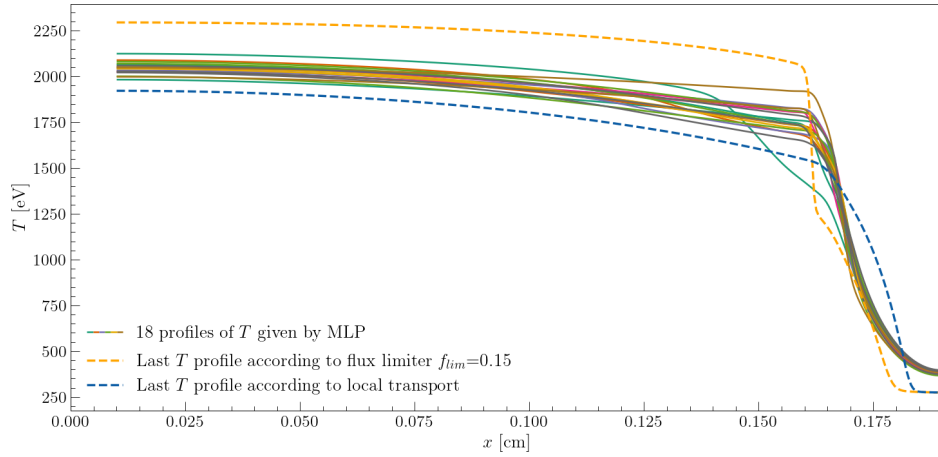


Figure 4.6: Comparison of the final profiles given by 18 separately trained MLPs

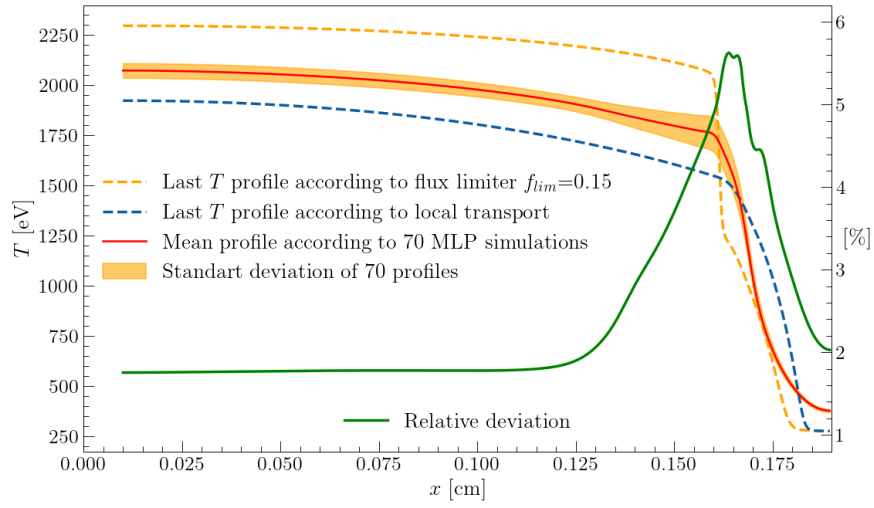


Figure 4.7: Deviation of the 70 separately trained MLPs

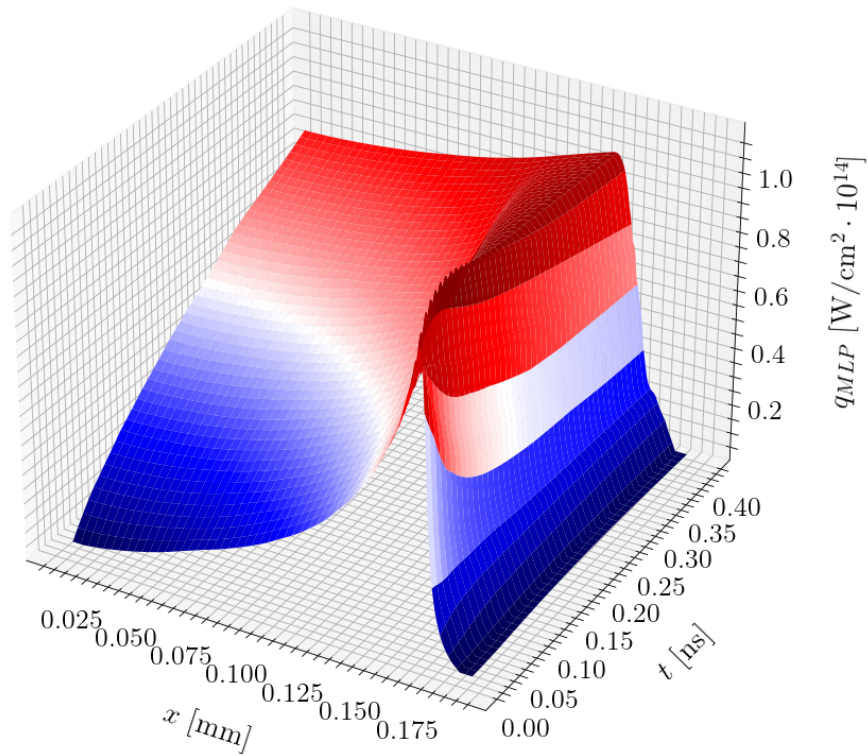


Figure 4.8: Time evolution of heatflux q_{MLP}



Chapter 5

Conclusions

So far there exist many hydrodynamics models developed in order to describe hot plasma with much less calculational effort than it is inevitable for kinetic approach. In this bachelor thesis I have presented our hydrodynamic model which is based on Multilayer Perceptron predicting the heatflux within plasma. The possibility of prediction of both heatflux inhibition and preheat with the help of relatively simple MLP were shown in chapter 4. The fact that our MLP model predicts the behavior of plasma parameters close to the kinetic models is rather impressive, but our model still suffers from a few imperfections such as the overestimation of heatflux in regions of low temperature gradient and general oscillations characteristic for artificial neural networks. This fact makes our MLP model a great tool for quick estimation of the heatflux but yet inapplicable in the case when high precision is required.

However the MLP can be relatively easily improved if the training process is enriched with significantly larger amount of kinetic simulations results residing not only in profiles of heatflux but also directly with α and β . The first could eliminate the problem of α definition from (3.10) without using the correction function (3.11), and the second may help to avoid the need to use self-similar solutions depicted in Fig 3.6.

In conclusion, it is necessary to note that our model must be further tested in order to be able to use it in practice. I'm going to devote my further research work to this aspect as part of my studies at our faculty.

During the preparation of this bachelor thesis, all the instructions listed in Bachelor Thesis Assignment were fulfilled.



Bibliography

- [1] D. T. Casey *et al.*, “Evidence of three-dimensional asymmetries seeded by high-density Carbon-ablator nonuniformity in experiments at the National Ignition Facility,” *Physical Review Letters*, vol. 126, no. 2, p. 025002, 2021.
- [2] A. L. Kritcher *et al.*, “Design of inertial fusion implosions reaching the burning plasma regime,” *Nature Physics*, vol. 18, no. 3, pp. 251–258, 2022.
- [3] H. Abu-Shawareb *et al.*, “Lawson criterion for ignition exceeded in an inertial fusion experiment,” *Physical Review Letters*, vol. 129, no. 7, p. 075001, 2022.
- [4] J. I. Castor, *Radiation Hydrodynamics*. Cambridge University Press, 2004.
- [5] D. Mihalas, “The equations of radiation hydrodynamics,” in *Astrophysical Radiation Hydrodynamics* (K.-H. A. Winkler and M. L. Norman, eds.), pp. 45–69, Dordrecht: Springer Netherlands, 1986.
- [6] M. Marinak *et al.*, “Three-dimensional HYDRA simulations of National Ignition Facility targets,” *Physics of Plasmas*, vol. 8, pp. 2275–2280, 2001.
- [7] R. J. Kingham and A. R. Bell, “An implicit Vlasov–Fokker–Planck code to model non-local electron transport in 2-D with magnetic fields,” *Journal of Computational Physics*, vol. 194, no. 1, pp. 1–34, 2004.
- [8] C. Lamy *et al.*, “Modeling of electron nonlocal transport in plasmas using artificial neural networks,” *Physical Review E*, vol. 105, 2022.
- [9] F. F. Chen, *Introduction to Plasma Physics and Controlled Fusion*. Springer Cham, 3 ed., 2016.

- [10] A. G. R. Thomas *et al.*, “A review of Vlasov-Fokker-Planck numerical modeling of inertial confinement fusion plasma,” *Journal of Computational Physics*, vol. 231, no. 3, pp. 1051–1079, 2012.
- [11] C. Mackrodt and H. Reeh, “Summational invariants,” *Journal of Mathematical Physics*, vol. 38, no. 6, pp. 3012–3019, 1997.
- [12] H. Milan, *Numerical Modeling Of Nonlocal Energy Transport In Laser-heated Plasmas*. PhD thesis, FJFI ČVUT v Praze, 2016.
- [13] R. M. More *et al.*, “A new quotidian equation of state (QEOS) for hot dense matter,” *Physics of Fluids*, vol. 31, no. 10, pp. 3059–3078, 1988.
- [14] A. Kemp and J. Meyer-ter-Vehn, “An equation of state code for hot dense matter, based on the qeos description,” *Nuclear Instruments and Methods in Physics Research Section A: Accelerators, Spectrometers, Detectors and Associated Equipment*, vol. 415, no. 3, pp. 674–676, 1998.
- [15] T. Heltemes and G. Moses, “Badger v1.0: A Fortran equation of state library,” *Computer Physics Communications*, vol. 183, no. 12, pp. 2629–2646, 2012.
- [16] S. P. Lyon and J. D. Johnson, “SESAME: The Los Alamos National Laboratory equation of state database.,” Tech. Rep. LA-UR-92-3407, Los Alamos National Laboratory, 1991.
- [17] Y. Igitkhanov and A. Pigarov, “Non-local transport effects on the tokamak SOL plasma parameters,” *Journal of Nuclear Materials*, vol. 176-177, pp. 557–561, 1990.
- [18] G. P. Schurtz, P. D. Nicolaï, and M. Busquet, “A nonlocal electron conduction model for multidimensional radiation hydrodynamics codes,” *Physics of Plasmas*, vol. 7, no. 10, pp. 4238–4249, 2000.
- [19] P. Kulhánek, *Úvod do teorie plazmatu*. Praha: AGA, 2011.
- [20] R. Kingham and A. Bell, “An implicit Vlasov–Fokker–Planck code to model non-local electron transport in 2-d with magnetic fields,” *Journal of Computational Physics*, vol. 194, no. 1, pp. 1–34, 2004.
- [21] A. G. R. Thomas, R. J. Kingham, and C. P. Ridgers, “Rapid self-magnetization of laser speckles in plasmas by nonlinear anisotropic instability,” *New Journal of Physics*, vol. 11, no. 3, p. 033001, 2009.
- [22] J. Nikl *et al.*, “Implicit reduced Vlasov–Fokker–Planck–Maxwell model based on high-order mixed elements,” *Journal of Computational Physics*, vol. 434, p. 110214, 2021.
- [23] A. S. Joglekar *et al.*, “Validation of OSHUN against collisionless and collisional plasma physics,” *Plasma Physics and Controlled Fusion*, vol. 60, no. 6, p. 064010, 2018.

- [24] M. Tzoufras *et al.*, “A Vlasov–Fokker–Planck code for high energy density physics,” *Journal of Computational Physics*, vol. 230, no. 17, pp. 6475–6494, 2011.
- [25] L. Spitzer and R. Härm, “Transport phenomena in a completely ionized gas,” *Physical Review*, vol. 89, pp. 977–981, 1953.
- [26] R. S. Cohen, L. Spitzer, and P. M. Routly, “The electrical conductivity of an ionized gas,” *Physical Review*, vol. 80, pp. 230–238, 1950.
- [27] D. L. Book, *NRL plasma formulary*. Washington, DC: Naval Research Lab., 1983.
- [28] J. F. Luciani, P. Mora, and J. Virmont, “Nonlocal heat transport due to steep temperature gradients,” *Physical Review Letters*, vol. 51, pp. 1664–1667, 1983.
- [29] “Welcome to PyTorch Lightning.” <https://pytorch-lightning.readthedocs.io/en/stable/>, 31 July 2023.
- [30] M. Lau and K. Hann Lim, “Review of adaptive activation function in deep neural network,” in *2018 IEEE-EMBS Conference on Biomedical Engineering and Sciences (IECBES)*, pp. 686–690, 2018.
- [31] S. Cuomo *et al.*, “Scientific Machine Learning through Physics–Informed Neural Networks: Where we are and what’s next,” *Journal of Scientific Computing*, vol. 92, p. 88, Jul 2022.
- [32] H. Choi *et al.*, “Real-time significant wave height estimation from raw ocean images based on 2d and 3d deep neural networks,” *Ocean Engineering*, vol. 201, p. 107129, 2020.
- [33] K. D. Humbird *et al.*, “Transfer learning to model inertial confinement fusion experiments,” *IEEE Transactions on Plasma Science*, vol. 48, no. 1, pp. 61–70, 2020.
- [34] K. D. Humbird and J. L. Peterson, “Transfer learning driven design optimization for inertial confinement fusion,” *Physics of Plasmas*, vol. 29, p. 102701, 10 2022.
- [35] M. D. Vander Wal *et al.*, “Transfer learning of high-fidelity opacity spectra in autoencoders and surrogate models,” *IEEE Transactions on Plasma Science*, vol. 51, no. 1, pp. 109–119, 2023.
- [36] M. D. Vander Wal *et al.*, “Transfer learning as a method to reproduce high-fidelity non-local thermodynamic equilibrium opacities in simulations,” *Journal of Plasma Physics*, vol. 89, no. 1, 2023.
- [37] X. Shi *et al.*, “Convolutional LSTM network: A machine learning approach for precipitation nowcasting,” in *NIPS*, 2015.
- [38] A. Vaswani *et al.*, “Attention is all you need,” 2023.

- [39] A. Dosovitskiy *et al.*, “An image is worth 16x16 words: Transformers for image recognition at scale,” 2021.
- [40] “ReLU- PyTorch 2.0 documentation.” <https://pytorch.org/docs/stable/generated/torch.nn.ReLU.html>, 31 July 2023.
- [41] “SGD - PyTorch 2.0 documentation.” <https://pytorch.org/docs/stable/generated/torch.optim.SGD.html>, 31 July 2023.
- [42] J. Brodrick *et al.*, “Testing nonlocal models of electron thermal conduction for magnetic and inertial confinement fusion applications,” *Physics of Plasmas*, vol. 24, p. 092309, 2017.
- [43] Ya. Zel’dovich and Yu. Raizer, *Physics of Shock Waves and High-Temperature Hydrodynamic Phenomena*. Dover Books on Physics, Dover Publications, 2012.
- [44] E. M. Epperlein and R. W. Short, “Nonlocal heat transport effects on the filamentation of light in plasmas,” *Physics of Fluids B: Plasma Physics*, vol. 4, no. 7, pp. 2211–2216, 1992.
- [45] J. Šilar, *Hydrodynamické modelování laserového plazmatu*. FJFI ČVUT v Praze, 2009.
- [46] A. Mote and M. Holec, “A surrogate model for ICF Thermal Flux Calculations,” Tech. Rep. LLNL-POST-851973, Lawrence Livermore National Laboratory, 2023.